Electronic Supplementary Material (ESI) for Journal of Materials Chemistry A.
This journal is © The Royal Society of Chemistry 2016

Electronic Supplementary Information (ESI)

General Synthesis of Graphene-Supported Bicomponent Metal Monoxides as Alternative High-Performance Li-Ion Anodes to Binary Spinel Oxides

Dong Wang,[a] Rui Zhang,[a] Jieying Li,[b] Xiaojing Hao,[b] Chunyan Ding,[a] Limin Zhao,[b] Guangwu Wen*[a,b,d], Jinping Liu*[c] and Weiwei Zhou,*[b]

[a]School of Materials Science and Engineering, Harbin Institute of Technology, Harbin 150001, China.

[b]School of Materials Science and Engineering, Harbin Institute of Technology at Weihai, Weihai 264209, China.

[c]School of Chemistry, Chemical Engineering and Life Science and State Key Laboratory of Advanced Technology for Materials Synthesis and Processing, Wuhan University of Technology, Wuhan, Hubei 430070, China.

[d]School of Materials Science and Engineering, Shandong University of Technology, Zibo 255000, China.

*Address correspondence to zhouweiwei@hit.edu.cn;g.wen@hit.edu.cn; liujp@whut.edu.cn

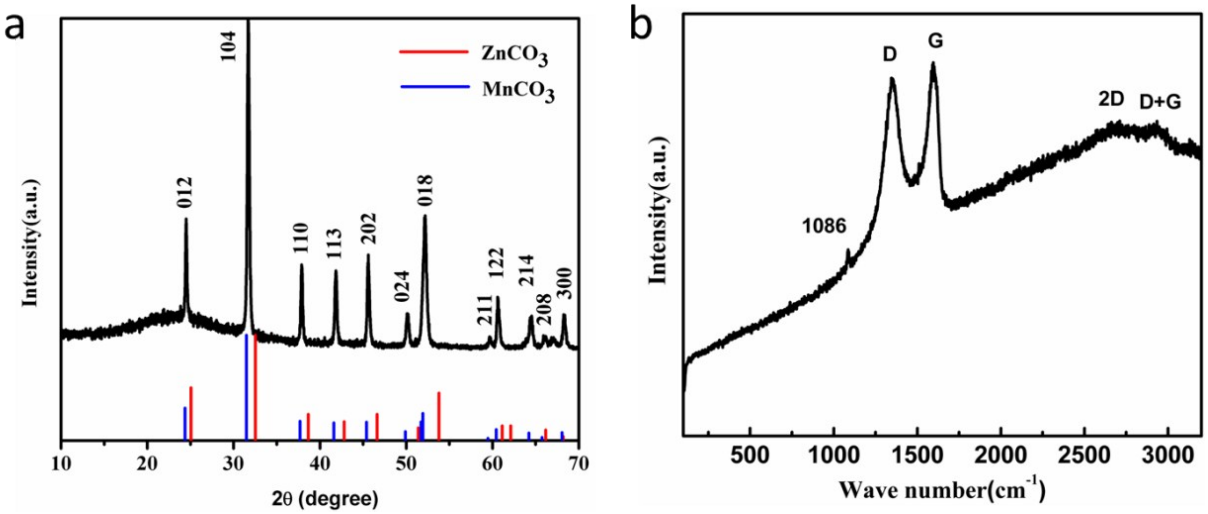

Fig. S1 (a) XRD pattern and (b) Raman spectrum of the as-prepared $Zn_xMn_{1-x}CO_3$/GF. Because of the same crystal structure and close solubility product constants of $ZnCO_3$ and $MnCO_3$, they would precipitate simultaneously. All the well-defined diffraction peaks could be attributed to $ZnCO_3$ (JCPDS card no. 08-0449) and $MnCO_3$ (JCPDS card no. 83-1763). In the Raman spectrum, the tiny peak at 1086 cm^{-1} is assigned to the symmetric C-O stretching (v_1), indicating the presence of $Zn_xMn_{1-x}CO_3$ in the composites. Two obvious peaks at 1595 cm^{-1} and 1365 cm^{-1} are attributed to G and D band of graphene, respectively.

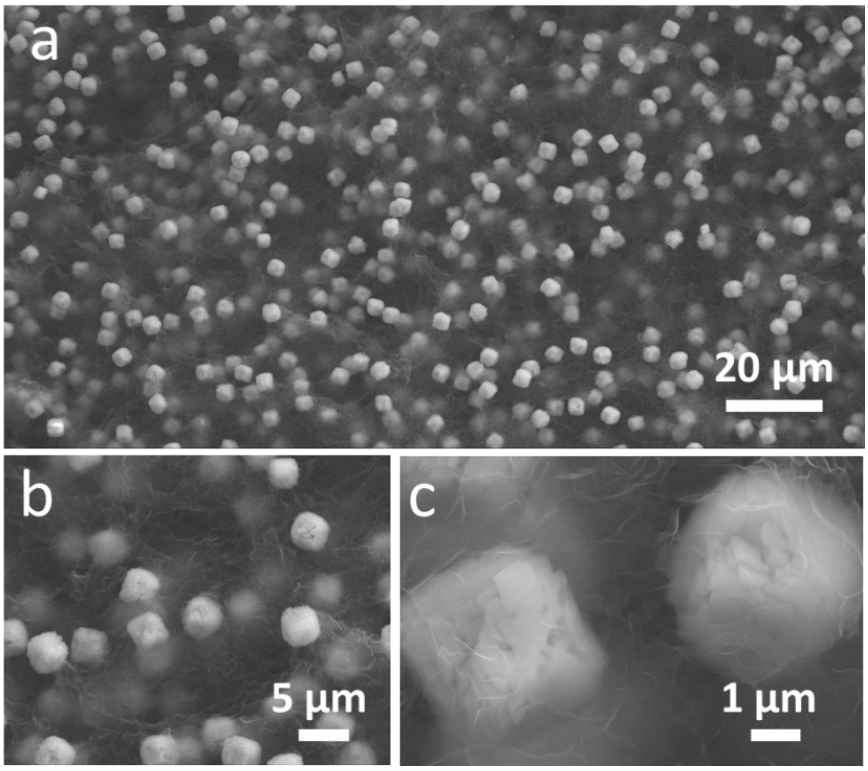

Fig. S2 Typical FESEM images of the as-prepared $Zn_xMn_{1-x}CO_3$/GF.

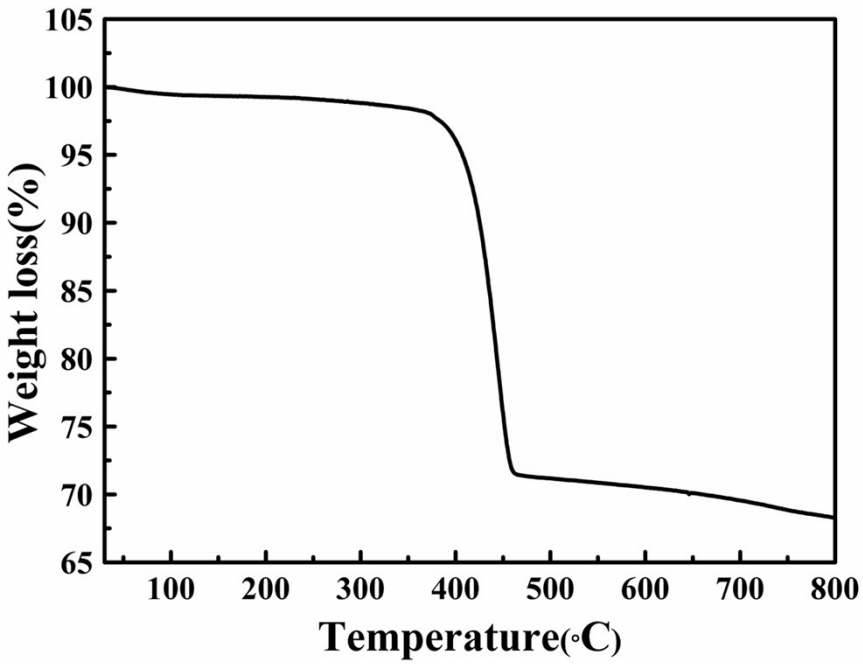

Fig. S3 TG curve of $Zn_xMn_{1-x}CO_3$/GF in inert atmosphere. The slight weight loss from room temperature to 200 °C is owing to the evaporation of absorbed water. The large weight loss between 200 °C to 600 °C is mainly due to the decomposition of $Zn_xMn_{1-x}CO_3$ as well as the further reduction of rGO. The $Zn_xMn_{1-x}CO_3$/GF precursor was annealed at the selected temperatures to investigate the composition evolution. Finally, 600 °C was chosen to completely transform the precursor into bicomponent metal oxides/GF.

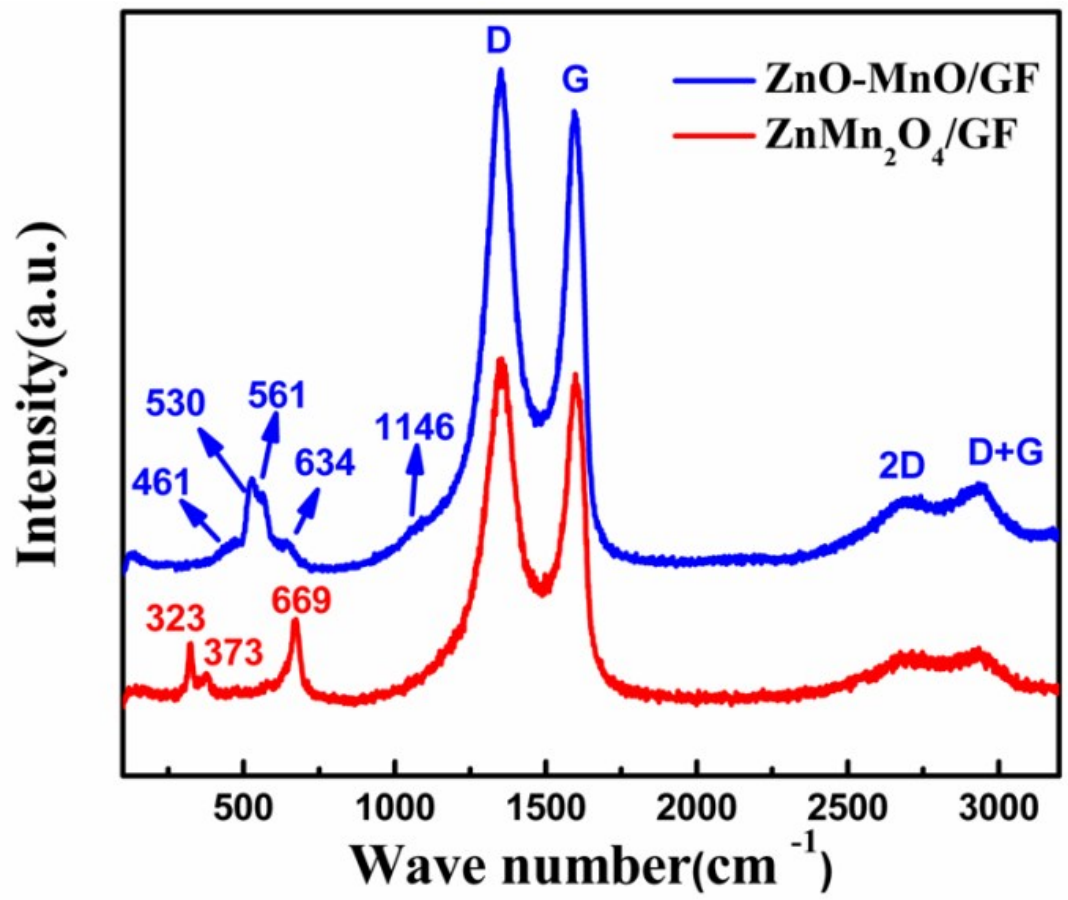

Fig. S4 Raman spectra of ZnO-MnO/GF and $ZnMn_2O_4$/GF. In the Raman spectrum of $ZnMn_2O_4$/GF, the three peaks at 323, 373 and 669 cm^{-1} are attributed to spinel $ZnMn_2O_4$.

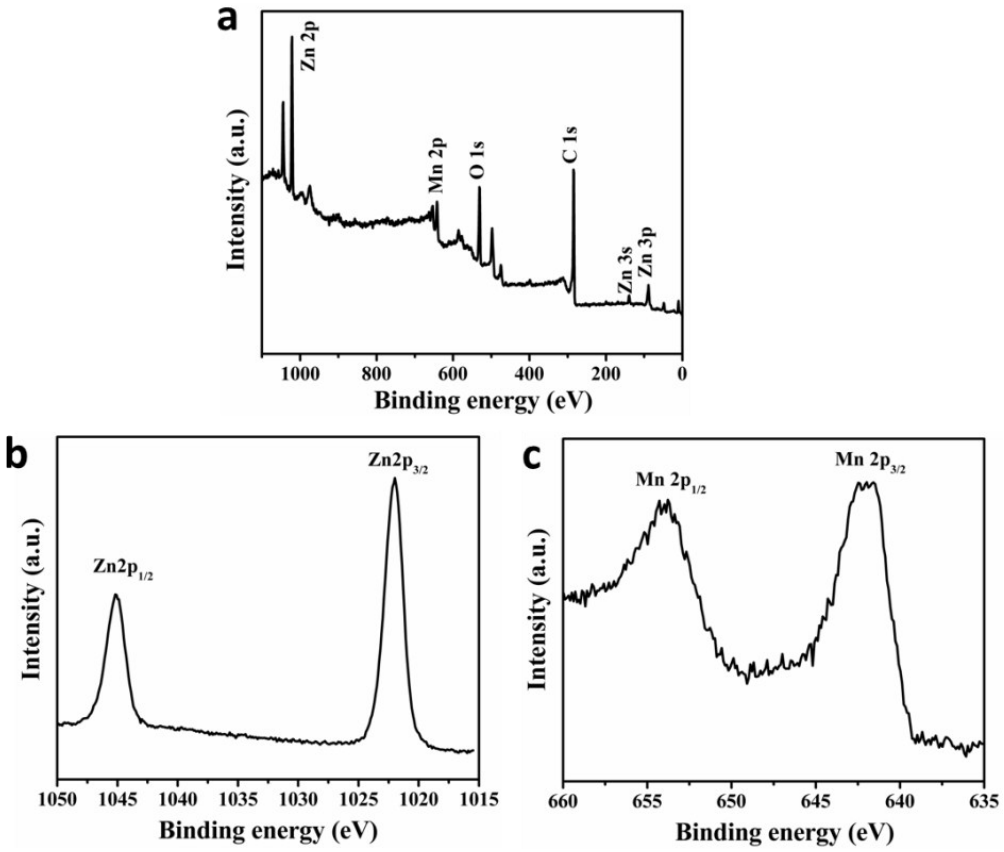

Fig. S5 XPS spectra for the ZnO-MnO/GF: (a) survey spectrum and high-resolution; (b) Zn 2p and (c) Mn 2p spectrum.

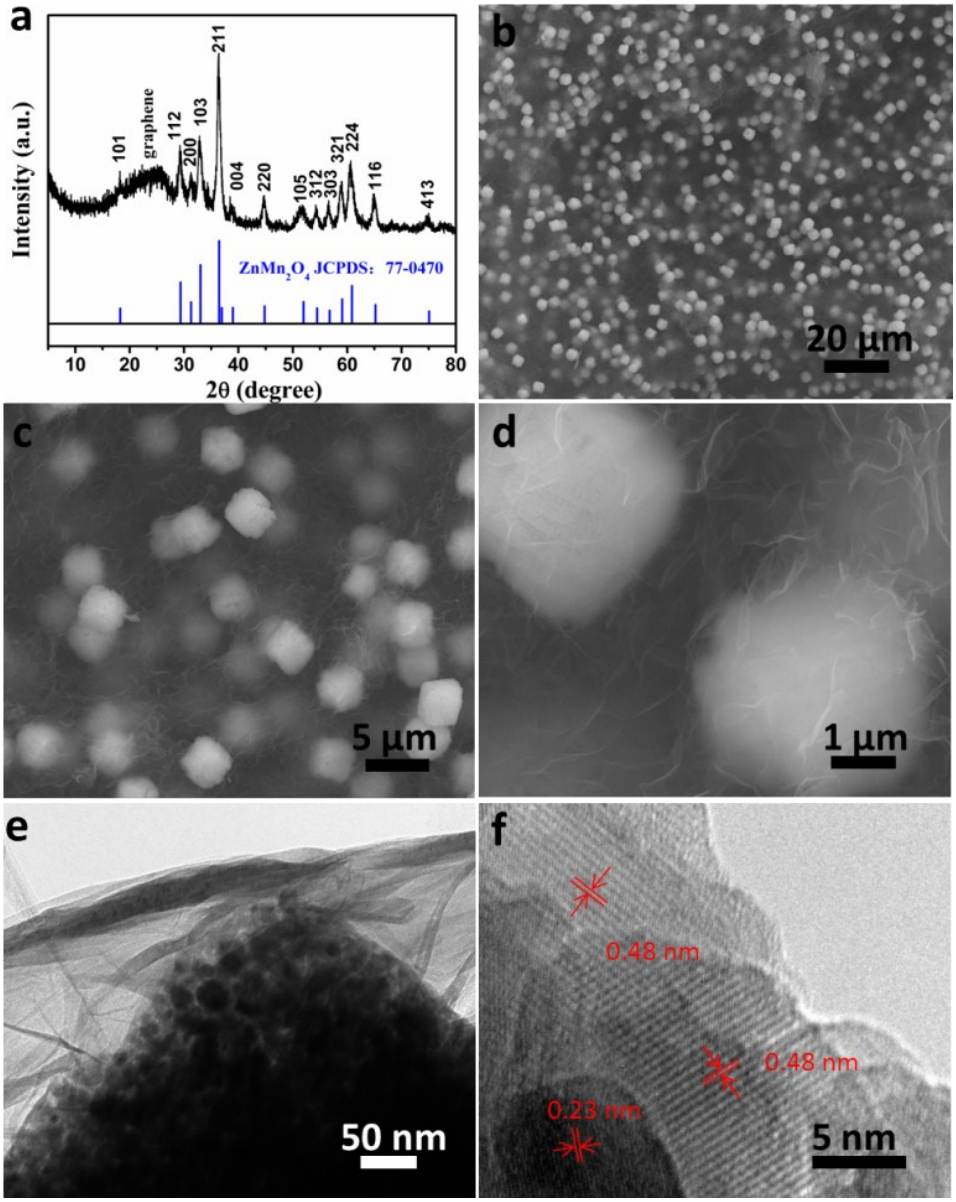

Fig. S6 Structure and morphology analyses of $ZnMn_2O_4$/GF: (a) XRD pattern; (b-c) typical FESEM images; (e) TEM image; (f) HRTEM image. The regular lattice fringes with interplanar spacings of 0.23 and 0.48 nm in (f) come from the (004) and (101) plane of spinel $ZnMn_2O_4$, respectively.

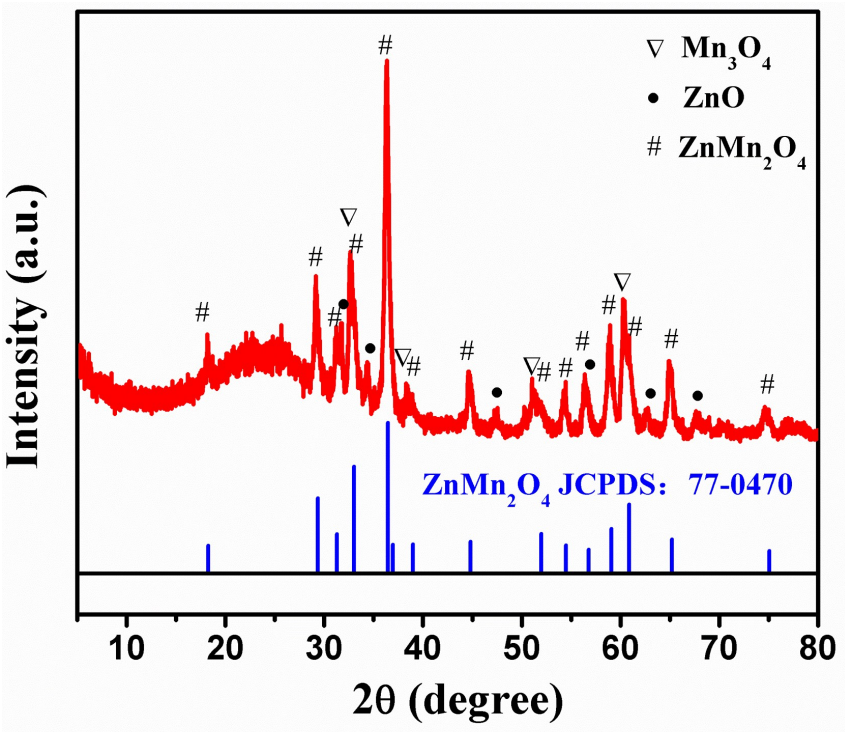

Fig. S7 XRD pattern of the product obtained by treating the $Zn_xMn_{1-x}CO_3$/GF hybrid at 520 °C.

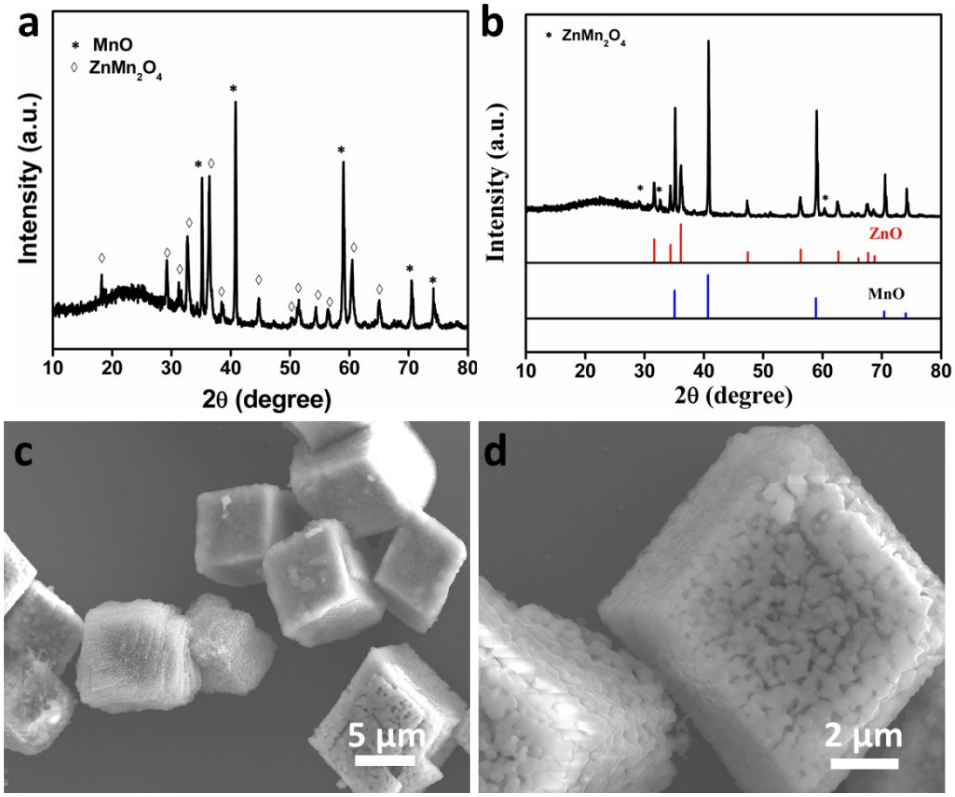

Fig. S8 XRD patterns of the products without adding graphene and annealed at: (a) 600 ºC and (b) 700 ºC. (c and d) FESEM images of the products without adding graphene and annealed at 700 ºC.

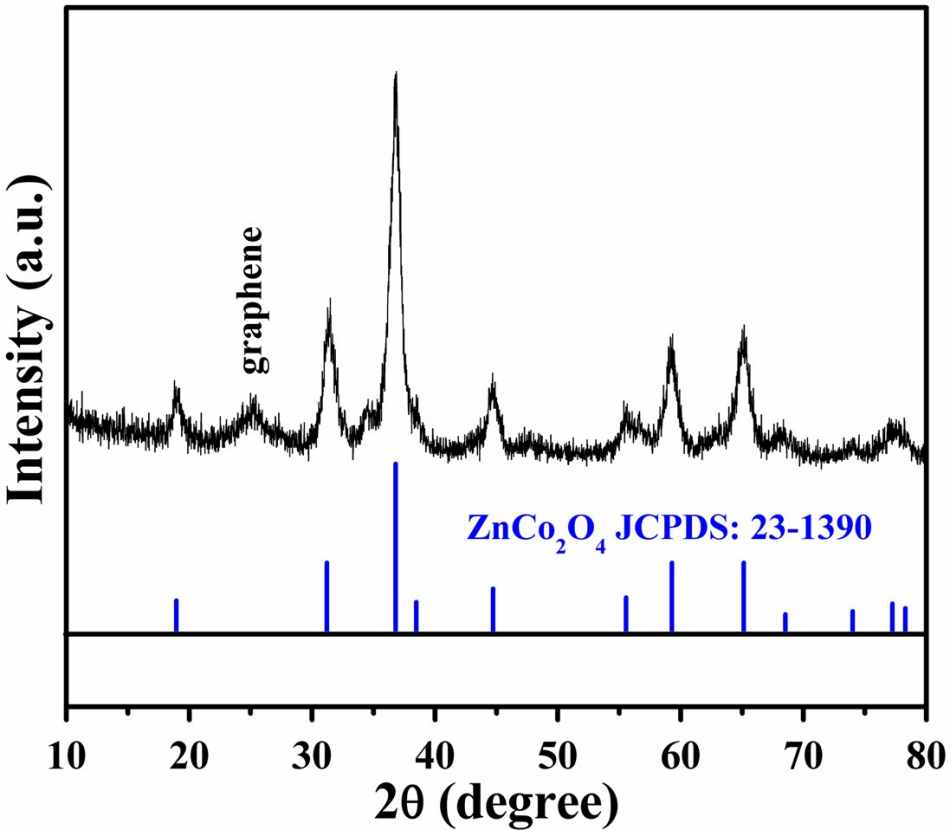

Fig. S9 XRD pattern of the calcination product of ZnCo-containing precursor/GF at 350 ºC.

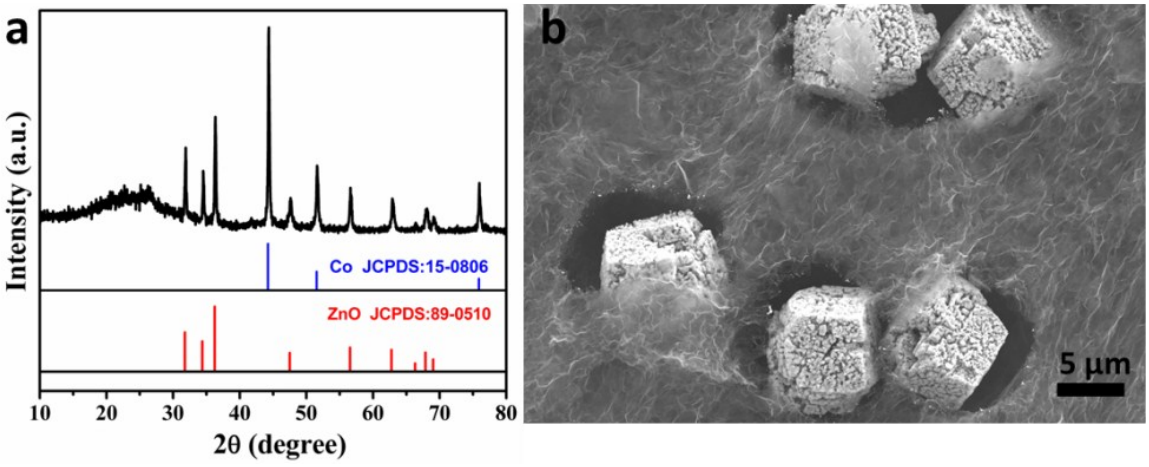

Fig. S10 (a) XRD pattern and (b) FESEM image of the calcination product of ZnCo-containing precursor/GF at 600 ºC. The voids between porous polyhedrons and graphene can be ascribed to the reaction of CoO with adjacent graphene at 600 °C.

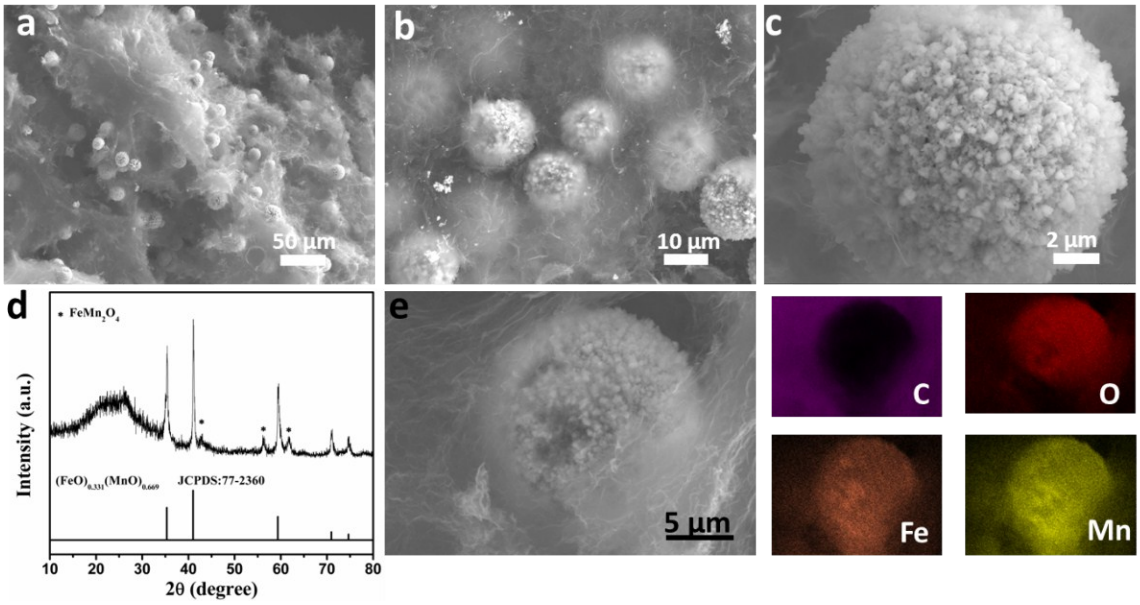

Fig. S11 Structural and morphology analyses of $(FeO)_{0.333}(MnO)_{0.667}$/GF. (a-c) typical FESEM images, showing that porous $(FeO)_{0.333}(MnO)_{0.667}$ microspheres are uniformly dispersed in the GF; (d) XRD pattern. The intense diffraction peaks are assigned to $(FeO)_{0.333}(MnO)_{0.667}$ (JCPDS card no. 77-2360). (e) STEM image and corresponding element mappings of C, O, Fe, and Mn.

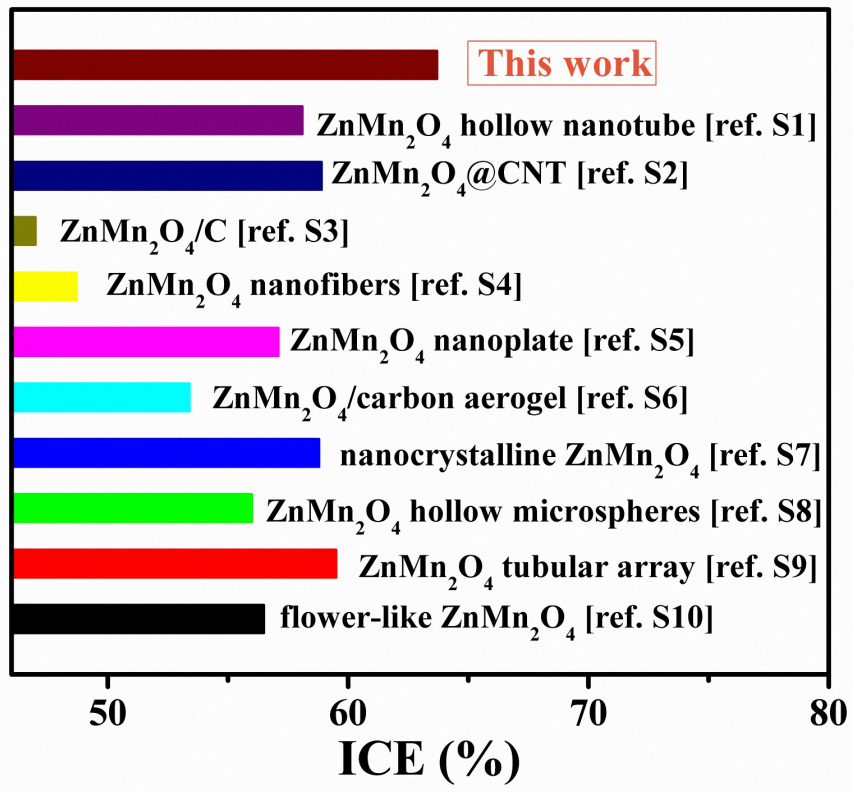

Fig. S12 Comparison of ICEs between our ZnO-MnO/GF electrode and other $ZnMn_2O_4$-based electrodes.

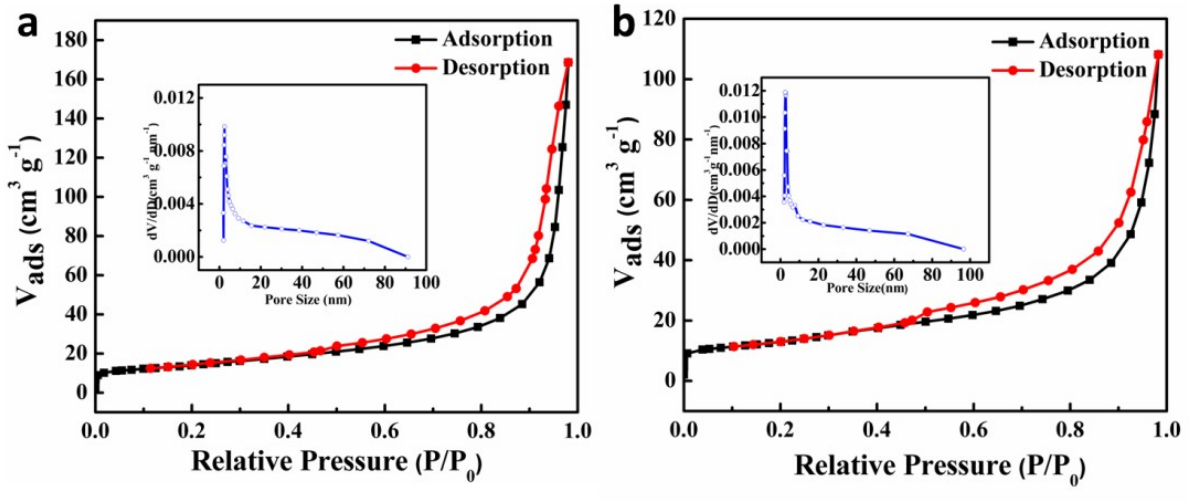

Fig. S13 Nitrogen adsorption-desorption isotherm and the corresponding pore size distribution curves of (a) $ZnMn_2O_4$/GF and (b) ZnO-MnO/GF. The ZnO-MnO/GF exhibits comparable specific surface area and similar pore size distribution to $ZnMn_2O_4$/GF.

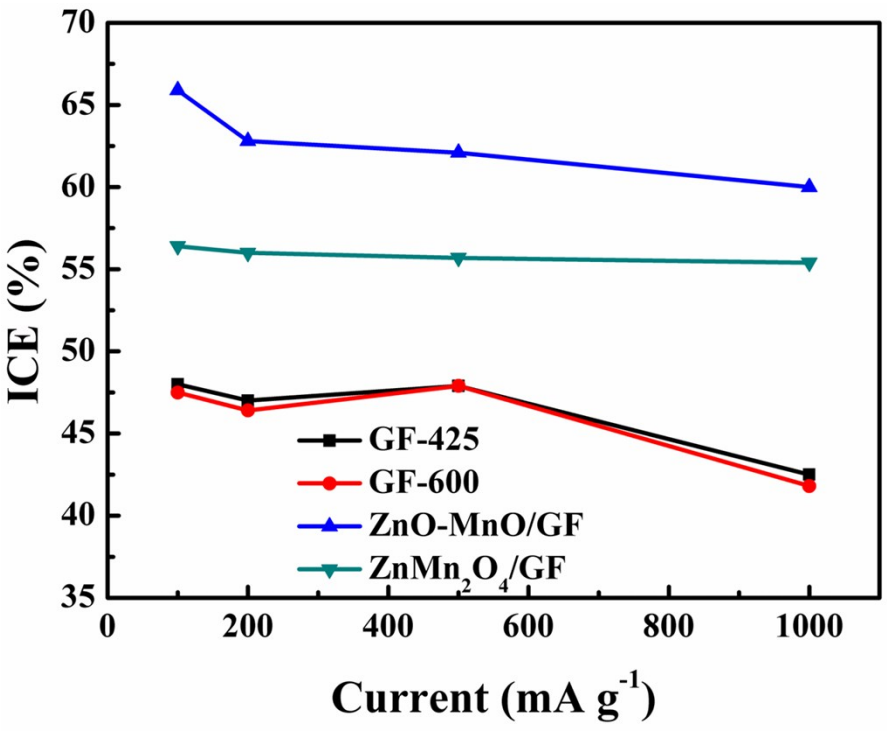

Fig. S14 Comparison of ICE at different current densities among GF-425, GF-600, ZnO-MnO/GF, and $ZnMn_2O_4$/GF electrodes.

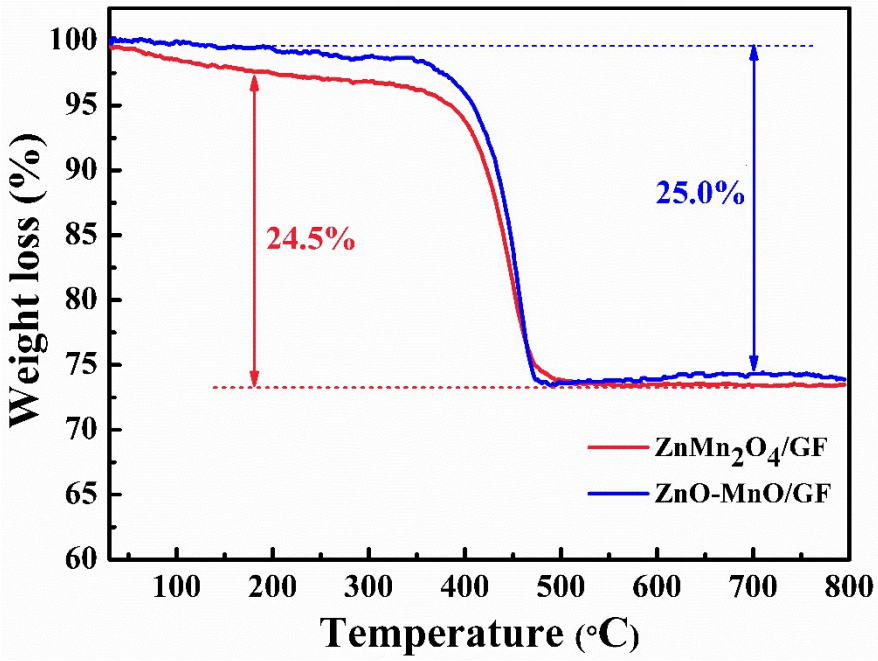

Fig. S15 TG curves of ZnO-MnO/GF and $ZnMn_2O_4$/GF hybrids, showing similar graphene content. According to previous studies, the final product of MnO after annealing at high temperature in air is Mn_2O_3.[S11] Based on the theoretical value (11.3 wt%) of weight gain from MnO to Mn_2O_3, the graphene content in the ZnO-MnO/GF is evaluated to be 30 wt%.

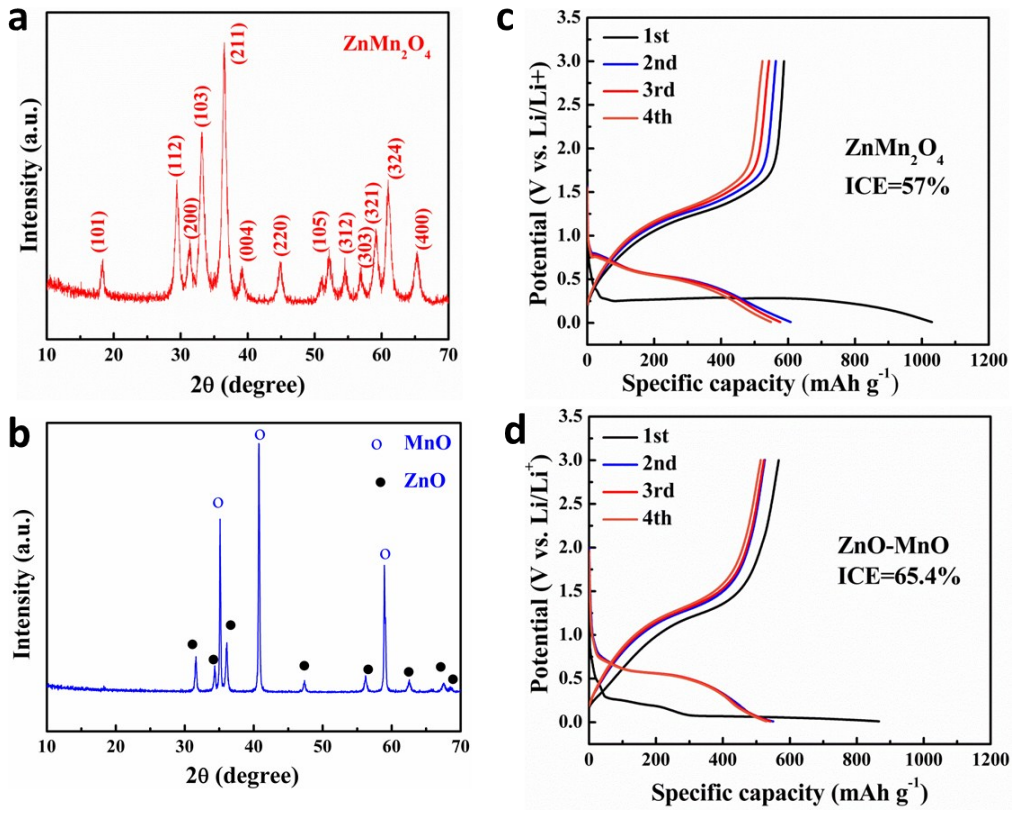

Fig. S16 (a and b) XRD patterns and (c and d) charge-discharge voltage profiles at 0.5 A g^{-1} of (a and c) pure $ZnMn_2O_4$ and (b and d) pure ZnO-MnO.

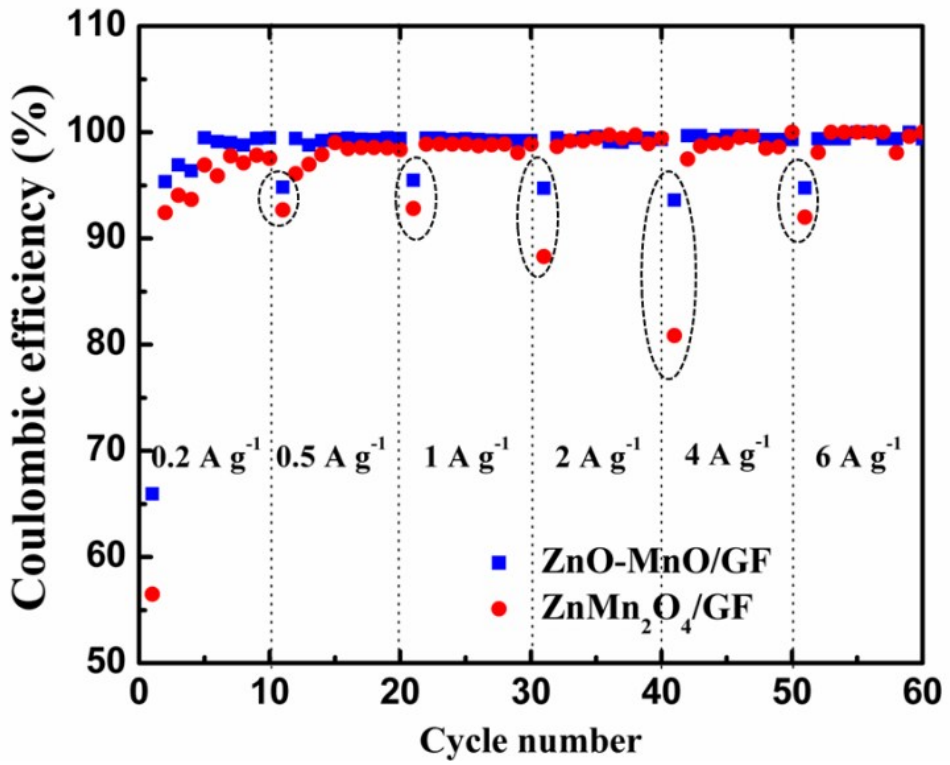

Fig. S17 Comparison of coulombic efficiency between ZnO-MnO/GF and $ZnMn_2O_4$/GF electrodes during current-changing cycling.

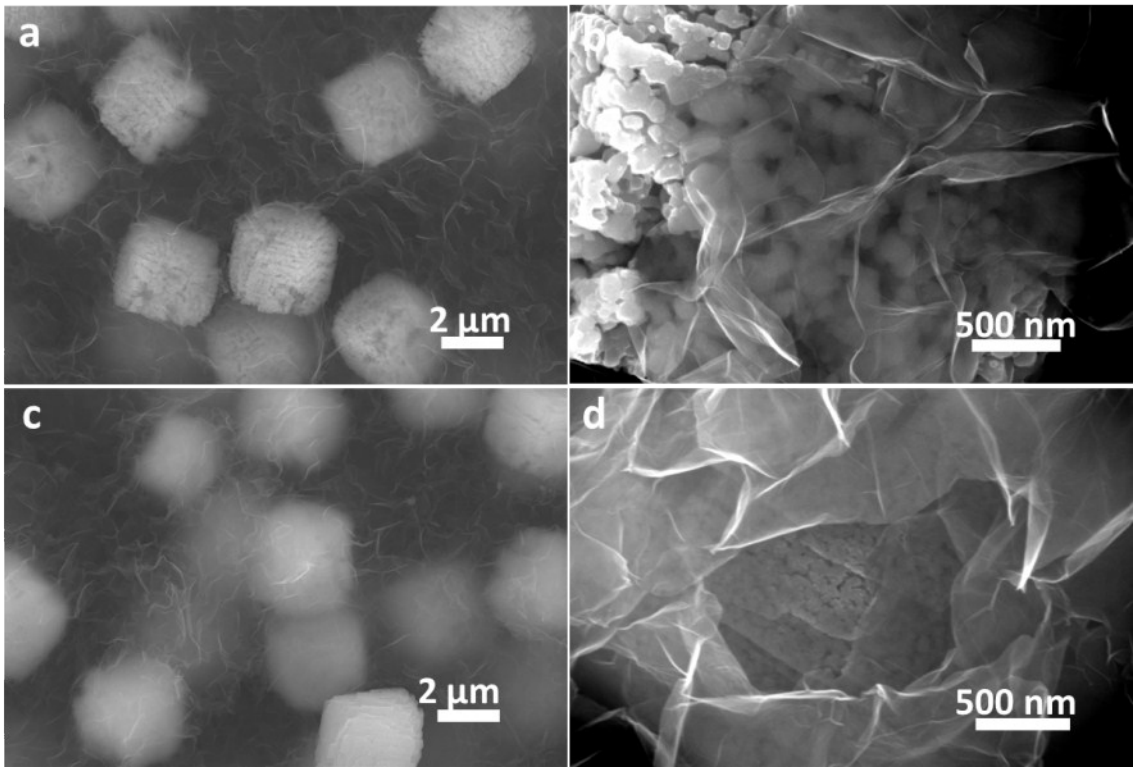

Fig. S18 Typical low- and high-magnification FESEM images of (a, b) ZnO-MnO/GF and (c, d) $ZnMn_2O_4$/GF, revealing that the ZnO-MnO/GF electrode possesses more porous structure than $ZnMn_2O_4$/GF, possibly due to more gases release and/or the re-crystallization of the MOs at high temperature.

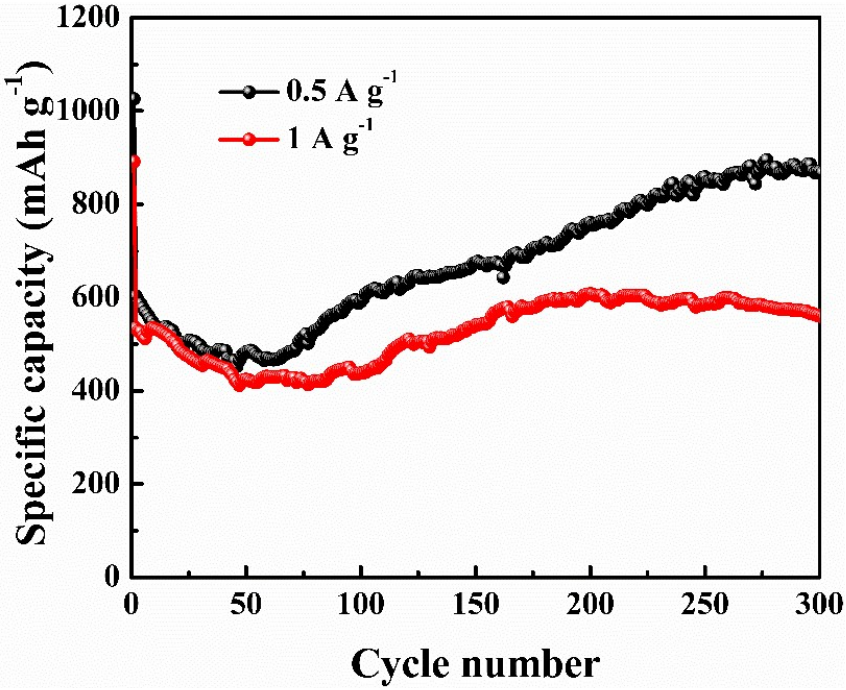

Fig. S19 Long-term cyclic performance of ZnO-MnO/GF electrode at 0.5 and 1 A g^{-1}. In both cases, the capacity increases gradually from about the 60th cycle.

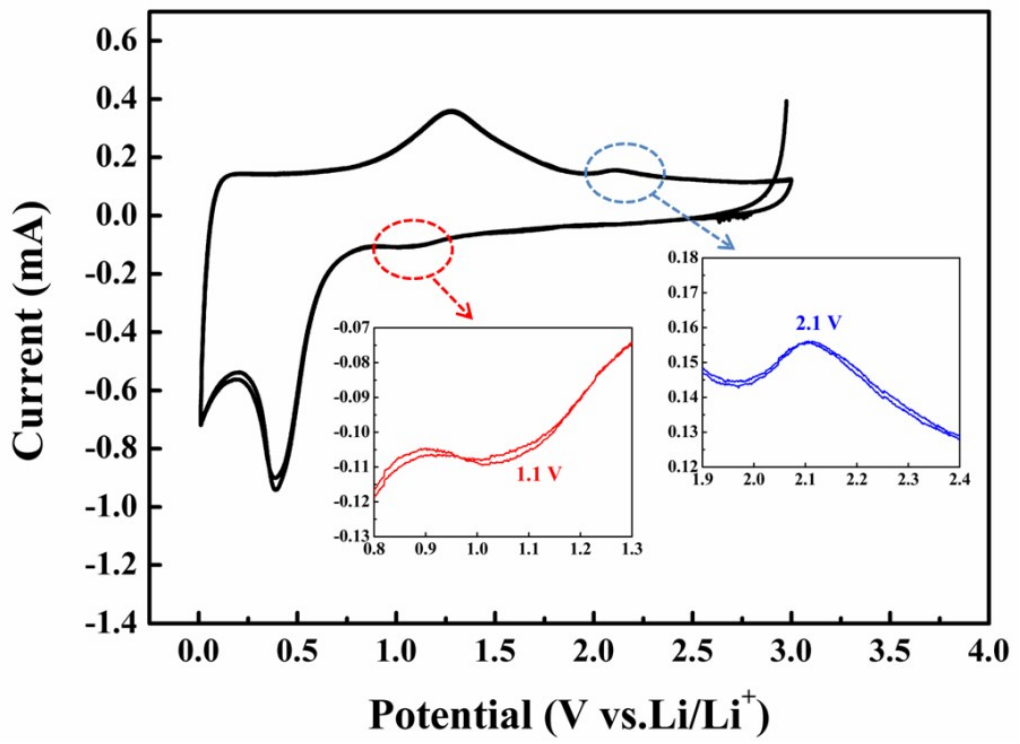

Fig. S20 CV of the ZnO-MnO/GF electrode after 150 charge/discharge cycles at 0.5 A g^{-1}. The minor oxidation peak at ~ 2.1 V is ascribed to Mn^{2+} to high valence Mn, while the reduction peak at 1.1 V is originated from the conversion of high valence Mn to Mn^{2+}.

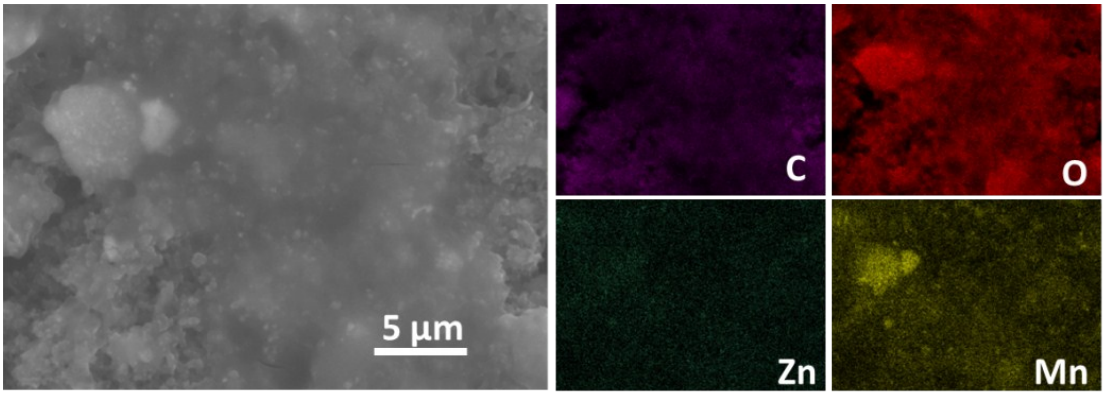

Fig. S21 STEM image and corresponding element mapping of C, O, Zn, and Mn in ZnO-MnO/GF electrode after 300 cycles at 0.5 A g^{-1}.

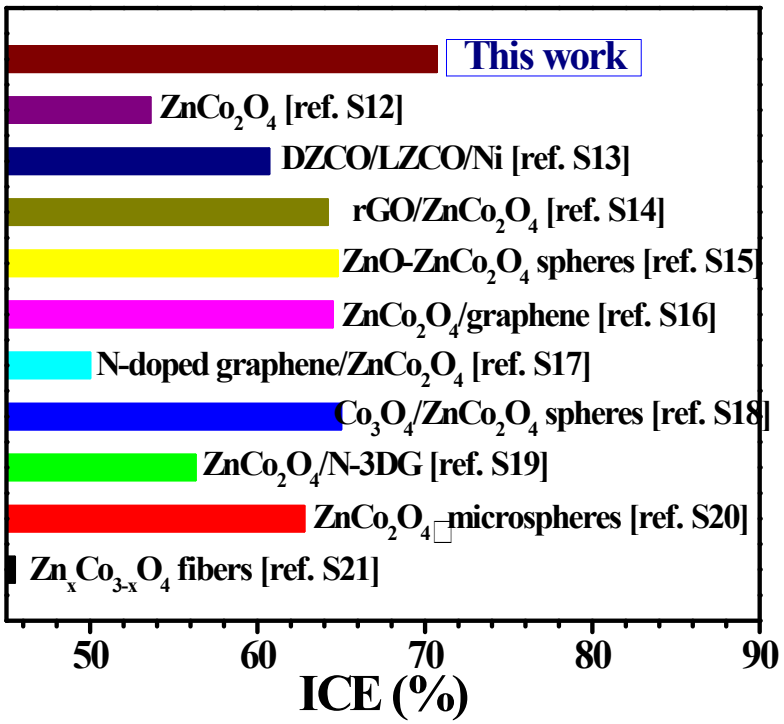

Fig. S22 Comparison of ICEs between our ZnO-CoO/GF electrode and other $ZnCo_2O_4$-based electrodes.

Reference

S1. L. H. Zhang, S. Q. Zhu, H. Cao, L. R. Hou and C. Z. Yuan, Chem. -Eur. J., 2015, 21, 10771-10777.
S2. W. Yao, J. G. Xu, J. Wang, J. H. Luo, Q. L. Shi and Q. Zhang, ACS Sustain. Chem. Eng., 2015, 3, 2170-2177.
S3. M. H. Alfaruqi, A. K. Rai, V. Mathew, J. Jo and J. Kim, Electrochim. Acta, 2015, 151, 558-564.
S4. P. F. Teh, Y. Sharma, Y. W. Ko, S. S. Pramana and M. Srinivasan, RSC Adv., 2013, 3, 2812-2821.
S5. J. Zhao, F. Wang, P. Su, M. Li, J. Chen, Q. Yang and C. Li, J. Mater. Chem., 2012, 22, 13328-13333.
S6. L. Yin, Z. Zhang, Z. Li, F. Hao, Q. Li, C. Wang, R. Fan and Y. Qi, Adv. Funct. Mater., 2014, 24, 4176-4185.
S7. Y. Yang, Y. Zhao, L. Xiao and L. Zhang, Electrochem. Commun., 2008, 10, 1117-1120.
S8. L. Zhou, H. B. Wu, T. Zhu and X. W. Lou, J. Mater. Chem., 2012, 22, 827-829.
S9. J. G. Kim, S. H. Lee, Y. Kim and W. B. Kim, ACS Appl. Mater. Interfaces, 2013, 5, 11321-11328.
S10. L. Xiao, Y. Yang, J. Yin, Q. Li and L. Zhang, J. Power Sources, 2009, 194, 1089-1093.
S11. Y. M. Sun, X. L. Hu, W. Luo, F. F. Xia and Y. H. Huang, Adv. Funct. Mater., 2012, 23, 2436-2444.
S12. C. C. Ai, M. C. Yin, C. W. Wang and J. T. Sun, J. Mater. Sci., 2004, 39, 1077-1079.
S13. H. Long, T. Shi, S. Jiang, S. Xi, R. Chen, S. Liu, G. Liao and Z. Tang, J. Mater. Chem. A, 2014, 2, 3741-3748.
S14. G. Gao, H. B. Wu, B. Dong, S. Ding and X. W. Lou, Adv. Sci., 2015, 2, 1400014.
S15. Q. Xie, D. Zeng, Y. Ma, L. Lin, L. Wang and D.-L. Peng, Electrochim. Acta, 2015, 169, 283-290.
S16. A. K. Rai and J. Kim, Solid State Sci., 2015, 48, 90-96.
S17. S. Sahoo, S. H. Bae, Y. S. Lee, J. M. Lee, J. M. Ahn, C. G. Kim and I. K. Oh, Carbon, 2015, 94, 455-463.
S18. Q. Wang, B. Yu, X. Li, L. Xing and X. Xue, J. Mater. Chem. A, 2016, 4, 425-433.
S19. F. Jiang, S. Zhao, J. Guo, Q. Su, J. Zhang and G. Du, Mater. Lett., 2015, 161, 297-300.
S20. D. Wang, X. Qi, H. Gao, J. Yu, Y. Zhao, G. Zhou and G. Li, Mater. Lett., 2016, 164, 93-96.
S21. Z. Xu, Y. Liu, W. Zhao, B. Li, X. Zhou and H. Shen, Electrochim. Acta, 2016, 190, 894-902.